Bioresources and Bioproducts

MDPI

Article

Pyrolysis Kinetics and Biochar Production of Almond and Pistachio Shells in a Fixed-Bed Pyrolyzer

Hamed M. El Mashad [1,2,*], Abdolhossein Edalati [1], Bor-Sen Chiou [3], Zach McCaffrey [3], Trung Cao [3], William Hart-Cooper [3], Ruihong Zhang [1] and Frank Mitloehner [4]

[1] Department of Biological and Agricultural Engineering, University of California, Davis, One Shields Ave., Davis, CA 95616, USA; ahedalati@ucdavis.edu (A.E.); rhzhang@ucdavis.edu (R.Z.)
[2] Agricultural Engineering Department, Mansoura University, El Gomhouria St., El Mansoura 35516, Egypt
[3] United States Department of Agriculture, Western Regional Research Center, 800 Buchanan Street, Albany, CA 94710, USA; bor-sen.chiou@usda.gov (B.-S.C.); zmccaffrey@gmail.com (Z.M.); trungcaoart@gmail.com (T.C.); william.hart-cooper@usda.gov (W.H.-C.)
[4] Department of Animal Science, University of California, Davis, One Shields Ave., Davis, CA 95616, USA; fmmitloehner@ucdavis.edu
* Correspondence: heelmashad@ucdavis.edu

Abstract

The effects of pyrolysis temperature (400–500 °C) and time (30–90 min) on the yield and chemical and physical properties of biochar produced from almond and pistachio shells were studied using a fixed-bed pyrolyzer. Thermogravimetric analysis (TGA) was employed to characterize the kinetics of thermal degradation of the shells. This study compared the thermal behavior observed by TGA with biochar yields obtained from a fixed-bed pyrolyzer, providing insight into the agreement between laboratory-scale thermogravimetric measurements and fixed-bed pyrolysis performance. Fourier transform infrared spectroscopy (FTIR) was performed for each type of biochar. Results showed higher biochar yields from almond shells (35.0–41.3% dry basis) than from pistachio shells (26.8–36.7% dry basis). Shell type, pyrolysis temperature, pyrolysis time, and their interactions had significant effects on biochar yield. The Derivative Thermogravimetric (DTG) profiles showed distinct thermal decomposition patterns for almond and pistachio shells. Almond shells exhibited broader decomposition regions, while pistachio shells showed more distinct decomposition stages. FTIR analysis of both shell biochars indicated reduced O–H and oxygen-containing groups with increasing pyrolysis temperature and residence time, suggesting greater carbonization, aromatic enrichment, and formation of carbonaceous compounds. Greater biochar yields were obtained from the fixed-bed pyrolyzer than from TGA. A first-order kinetics model adequately described the thermal decomposition of both shell types. Apparent activation energies were 41.83–44.99 kJ mole^{-1} for almond shells and 58.19–63.58 kJ mole^{-1} for pistachio shells. Model validation showed a good agreement between the experimental and predicted conversion values. The results provide a basis for evaluating the potential of TGA-derived thermal behavior to inform biochar production conditions in fixed-bed pyrolysis.

Keywords: thermochemical processes; sustainable agriculture; activation energy; nut shells; biomass valorization

Academic Editor: Yukesh Kannah Ravi

Received: 11 July 2026
Revised: 16 August 2026
Accepted: 18 August 2026
Published: 20 August 2026

1. Introduction

California is the main producer of almonds and pistachios in the US, with the industries generating 451,000 tons of almond shells and 180,000 tons of pistachio shells as

byproducts every year. These amounts of shells were estimated based on crop yields in 2022 [1] and shell yields of 22% and 45% for almond and pistachio, respectively. These byproducts create an economic and environmental burden for their disposal but also opportunities for new coproducts to improve overall sustainability. Identifying new markets for shell utilization will foster the economic viability and sustainability of nut production. Almond and pistachio shells have been used as boiler fuel or feedstock for gasification and production of biochar and activated carbon [2]. The nut industry continues to search for higher-value and more sustainable uses of shells and other byproducts to achieve zero waste in orchards and sustainable nut production. Production of biochar from nut wastes will increase their value and reduce their negative environmental impacts, such as emissions of greenhouse gases resulting from uncontrolled degradation. Biochar production from nut shells provides an opportunity to improve soil quality, sequester carbon, and reduce environmental impacts associated with waste degradation [3].

Thermogravimetric analysis (TGA) has been applied to understand the thermal stability and decomposition profile of biomass under different temperatures and times. The resulting mass-loss profiles provide information about biomass decomposition behavior and potential biochar production under different pyrolysis conditions. Debevc et al. [4] performed thermogravimetric analyses of raw and carbonized almond shell samples. The derivative curves (DTG) are used to clearly observe the small changes in weight of the samples. Results showed that 15% weight loss was observed between 200 and 300 °C for almond shells. This was attributed to the decomposition of hemicellulose. A drastic decrease in weight was determined at 340 °C, which was attributed to the degradation of cellulose and lignin. McCaffrey et al. [5] conducted thermogravimetric analyses of almond shells using argon as an inert gas. Results showed that the main decomposition occurred over a temperature range from 200 °C to 450 °C with a char (fixed carbon plus ash) yield of 24.4%. However, pyrolysis kinetics were not studied.

Fixed-bed reactors are commonly used in small-scale biomass pyrolysis because of their simple design, low operating cost, and stable performance. They can handle feedstocks with uniform particle size and limited fine particles (e.g., [6]). In our previous study [7], almond shells were used to produce biochar using a fixed-bed pyrolyzer at different temperatures and times. Biochar yield was significantly affected by temperature and time. The highest biochar yields were obtained at a pyrolysis temperature of 300 °C and pyrolysis times of 30 and 60 min. Higher temperatures also resulted in biochar with higher particle density and pH. However, the pyrolysis kinetics were not studied. Moreover, the yield of biochar from TGA was not compared with that from a fixed-bed pyrolyzer. Gezahegn et al. [8] mentioned that the increase in pyrolysis temperature resulted in a reduction in acidic organic compounds and the concentration of alkaline earth metals (particularly Ca and Mg) as the organic fraction is volatilized. Açıkalın et al. [9] studied the pyrolysis of pistachio shells in a fixed-bed reactor under different temperatures and times. Results showed that biochar yield was not affected by reaction time but was mainly controlled by temperature. Debevc et al. [4] determined the yield and properties of almond shell biochar at three different temperatures: 300, 500, and 700 °C. Results showed that the pyrolysis at 700 °C increased carbon content from 47% in almond shells to 75% in biocarbon. The biocarbon produced at higher temperatures has improved thermal stability than that produced at lower temperatures. Also, the electrical conductivity of biocarbon produced at 700 °C was 53 times higher than that produced at 500 °C.

Determination of pyrolysis kinetics is important for understanding the behavior of a feedstock during thermal decomposition to optimize pyrolysis conditions, predict the yields of pyrolysis products, and design and scale-up pyrolysis reactors [10]. Shrivastava et al. [11] reported that biomass pyrolysis kinetics can be evaluated using both model-fitting and

model-free (i.e., iso-conversional) methods. Model-fitting approaches involve assuming a reaction model that best describes the experimental data and estimating the corresponding kinetic parameters. They may be applied to single or multiple thermogravimetric analysis (TGA) curves depending on the modeling framework. In contrast, model-free methods determine the apparent activation energy as a function of conversion by analyzing data obtained at multiple heating rates [12]. Although model-fitting methods are widely used due to their simplicity, they may introduce bias in kinetic parameters when an inappropriate reaction model is assumed, particularly under non-isothermal conditions [13]. Despite this limitation, model-fitting approaches provide explicit kinetic rate expressions that can be used for process modeling and reactor simulations [14].

TGA can be used to measure the changes in the mass of a sample during heating or at a constant temperature and under controlled atmospheres such as nitrogen. TGA has been widely used to study the thermal decomposition kinetics of various biomass materials, including agricultural residues and woody biomass [10,14–17]. Khan et al. [18] investigated almond shell pyrolysis for bioenergy applications using thermogravimetric analysis conducted from ambient temperature up to 900 °C under an inert atmosphere at different heating rates. Kinetic parameters were determined using iso-conversional model-free methods, including the Friedman, Ozawa–Flynn–Wall (OFW), and Kissinger-Akahira-Sunose (KAS) approaches. Artificial neural networks (ANN) and boosted regression trees (BRT) were employed to predict activation energy. The results showed that comparable activation energy values were obtained across different conversion levels using the applied models.

To the best of our knowledge, no previous study has compared biochar yields from almond and pistachio shells obtained by TGA and a fixed-bed pyrolyzer under comparable conditions. In addition, although some studies have investigated the pyrolysis of almond and pistachio shells, there remains a lack of research on the pyrolysis kinetics of these materials. These research gaps limit the reliability of TGA-based yield predictions and necessitate validation under practical pyrolysis conditions. Understanding the kinetics of pyrolysis can aid in optimizing pyrolysis conditions and scaling up pyrolyzers. Therefore, the goal of this research was to valorize almond and pistachio shells to produce biochar that can be used as a soil amendment and for other environmental applications. The research objectives were to (1) compare the yield of biochar from a fixed-bed pyrolyzer with that determined from a thermogravimetric analyzer; (2) study the effects of pyrolysis conditions on almond and pistachio shell biochar yields and properties using a fixed-bed pyrolyzer; and (3) determine the kinetics of thermal decomposition of the almond and pistachio shells. Comparing the yields of biochar from TGA and a fixed-bed pyrolyzer is important for designing pyrolyzers suitable for farm applications.

2. Materials and Methods

2.1. Collection of Almond and Pistachio Shells

Almond and pistachio shells were collected from commercial processors in Merced County, California. Almond and pistachio shells were each collected as a single batch during the 2021 and 2023 harvest seasons. The materials were stored under ambient conditions, in closed plastic drums, until used in the experiments in 2024. The specific varieties were not known; however, the samples were most likely composed of mixed varieties.

2.2. Thermogravimetric Analysis (TGA)

Thermogravimetric analysis was performed using a Mettler Toledo TGA/DSC3+ (Columbus, OH, USA) and 150-µL crucibles without lids. The average masses of the shells used in the tests were 17.5 and 23.4 mg for almond and pistachio shells, respectively. The shells were ground using an IKA MF10 Microfine Grinder (IKA-Werke GmbH & Co. KG,

Staufen, Baden-Württemberg, Germany) equipped with a 1.5 mm screen prior to TGA. For mass-loss analysis, the heating program ramped from room temperature to 500 °C at 10 °C min^{-1} with a constant nitrogen flow rate of 50 mL min^{-1}. The furnace and samples were purged with N for 10 min prior to heating. The thermogravimetric curves were plotted as the remaining mass percentage as a function of temperature. The heating rates in each TGA test were 5 K min^{-1} (0.08 K s^{-1}), 10 K min^{-1} (0.17 K s^{-1}), and 20 K min^{-1} (0.34 K s^{-1}) for almond and pistachio shells. A constant nitrogen flow rate of 50 mL min^{-1} was applied in all tests. Measurements were performed in triplicate, and analysis used buoyancy correction. The TGA is calibrated approximately once per year by a Mettler Toledo technician.

2.3. Kinetics of Pyrolysis

The decomposition of biomass material can be described by the following kinetic equation [10,19]:

$$\frac{dX}{dt} = k(T)f(X) \tag{1}$$

where X is the degree of the sample decomposition over the pyrolysis time (t, s). The degree of the sample decomposition (i.e., degree of conversion) can be determined as follows [20]:

$$X = \frac{X_0 - X_t}{X_0 - X_f} \tag{2}$$

where X_0 is the initial mass, X_t is the instantaneous mass at time t, and X_f is the residual mass at the end of each test at 500 °C.

$k(T)$ is a temperature-dependent rate constant that can be calculated based on the Arrhenius law [21]:

$$k(T) = Ae^{\frac{-E_a}{RT}} \tag{3}$$

where A is the frequency factor (s^{-1}), E_a is the apparent activation energy (J mol^{-1}), R is the universal gas constant (8.3145 J mol^{-1} K^{-1}), and T is temperature (K).

The conversion function ($f(X)$) can be expressed as a simple reaction model for calculating the remaining mass fraction in a single-step process [22]:

$$f(X) = (1 - X)^n \tag{4}$$

where n is the reaction order. Substituting the values of $k(T)$ and $f(X)$ in Equation (1):

$$\frac{dX}{dt} = Ae^{\frac{-E_a}{RT}}(1 - X)^n \tag{5}$$

For a non-isothermal pyrolysis process, the temperature of the sample changes over the pyrolysis time. The degree of sample decomposition changes with temperature and can be expressed as follows [19]:

$$\frac{dX}{dT} = \frac{dX}{dt}\frac{dt}{dT} \tag{6}$$

dT/dt is the heating rate (β). Therefore, Equation (5) becomes:

$$\frac{dX}{dT} = \frac{A}{\beta}e^{\frac{-E_a}{RT}}(1 - X)^n \tag{7}$$

It should be mentioned that different values of n (0.0–6.0) were reported in the literature (e.g., [10,23]) for different biomass and other materials. However, as mentioned by Wang et al. [10], a pseudo-order ($n \neq 1$) has no physical meaning, even if it improves the fitting of the model parameters. Therefore, in this study, a first-order kinetic reaction was

assumed, and the values of A and E_a were estimated and reported. Fischer et al. [14] evaluated different kinetic approaches for several biomass types and found that order-based reaction models were among the most appropriate, with the first-order model giving the lowest RMSD for several biomass samples.

Two replicates of the TGA tests were used for parameter estimation, and a third independent run was used for validation. The values of activation energy (E_a) and frequency factor (Log A) could be estimated by using different methods, such as a model-free method and a model-fitting method [10]. In this study, the kinetic parameters (A and E_a) were estimated using the fminsearch function in GNU Octave version 10.1.0 [24]. A function was developed to minimize the differences between the experimental and predicted values of the degree of conversion at different temperatures by adjusting the kinetics parameters. The predicted values were estimated by solving the differential equation using the ODE45 function with initial guesses of the kinetic parameters (A and E_a). The parameters were estimated using the data collected in the temperature range of 150 to 500 °C. The changes of less than 5% mass at temperatures lower than 150 °C were not included in the analysis since these were attributed to vaporization of moisture [10,25].

2.4. Biochar Production in a Fixed-Bed Pyrolyzer

Biochar was produced from almond and pistachio shells in a fixed-bed kiln at controlled temperatures. A factorial experimental design with three pyrolysis temperatures (400, 450, and 500 °C) and three residence times (30, 60, and 90 min) was applied. Each treatment combination was conducted in duplicate. Pyrolysis temperatures and residence times were selected based on previous studies and to represent practical fixed-bed processing conditions for evaluating effects on biochar yield, carbonization, and physicochemical properties. Temperatures below 400 °C may result in incomplete carbonization and greater volatile retention, whereas temperatures above 500 °C generally promote further devolatilization, lower biochar yield, and higher energy requirements. The selected temperatures have been reported to produce suitable biochars from agricultural residues [26,27], while the studied residence times represent short and extended pyrolysis durations.

Crucibles made of graphite (crucible number 6, McMaster-Carr, Santa Fe Springs, CA, USA) covered with porcelain covers were used as pyrolysis reactors. Two crucibles were used for each type of shell. A manifold for nitrogen distribution into the containers was designed and fabricated (Figure 1). The manifold supplied nitrogen simultaneously to the four crucibles from the bottom, with the same nominal flow path provided to each crucible (Figure 1). However, the actual flow rate through each individual crucible was not independently measured or verified. Two hundred grams (wet basis (w.b.)) of shells were used without grinding in each crucible. No additional packing was applied to the shells; therefore, the packing density was expected to be similar to the bulk density reported in Table 1. Particle-size distribution was not measured in this study. After loading the shells into crucibles, each crucible was covered with a tile to prevent the contact of the shells from contacting the gas inside the kiln cavity. The tiles were not completely sealed, allowing pyrolysis vapors to escape. Thus, the covers reduced direct atmospheric exposure but did not substantially restrict vapor release.

Before starting the heating program in the kiln, the kiln cavity was purged with nitrogen at a rate of 47.2 L min^{-1} for 10 min to ensure inert conditions. Then the nitrogen flow rate was reduced to 9.44 L min^{-1} and maintained until the end of pyrolysis. During pyrolysis, the chamber and material temperatures were measured using K-type thermocouples. Temperatures were continuously recorded using a Hobo data logger. Examples of recorded temperatures of biomass are shown in Figure 2.

Figure 1. Shells in crucibles housed in the kiln.

Table 1. Chemical composition of almond and pistachio shells.

Parameters	Almond Shells	Pistachio Shells
Organic N, % N	0.82 ± 0.01 **	0.18 ± 0.01
Ammonium, % N	0.02 ± 0.00	ND ***
Total N, % N	0.84 ± 0.00	0.18 ± 0.00
Phosphorus, % P_2O_5	0.19 ± 0.04	0.07 ± 0.02
Potassium, % K_2O	2.96 ± 0.35	0.13 ± 0.01
Sulfur, % S	0.05 ± 0.00	0.02 ± 0.00
Calcium, % Ca	0.37 ± 0.06	0.04 ± 0.00
Magnesium, % Mg	0.10 ± 0.01	0.02 ± 0.00
Sodium, % Na	0.04 ± 0.00	0.04 ± 0.01
Zinc, ppm Zn	22.40 ± 9.90	2.40 ± 0.57
Iron, ppm Fe	693.50 ± 496.95	7.90 ± 1.27
Manganese, ppm Mn	20.25 ± 3.32	0.75 ± 0.21
Copper, ppm Cu	7.25 ± 1.77	0.95 ± 0.35
Boron, ppm B	62.85 ± 6.72	1.55 ± 0.35
Soluble salts, mS/cm	24.50 ± 0.98	1.44 ± 0.11
pH	4.95 ± 0.07	5.10 ± 0.00
Moisture, % *	7.4 ± 0.20	5.90 ± 0.20
Dry matter, % *	92.60 ± 0.20	94.10 ± 0.20
Volatile solids, % *	86.70 ± 2.10	93.20 ± 0.30
Ash, % *	5.80 ± 2.10	0.90 ± 0.20
Total carbon, % C	44.99 ± 1.00	48.75 ± 0.23
Total C/N ratio	53.55 ± 1.20	270.80 ± 1.27
Bulk density, kg/m^3 *	269.76 ± 3.69	377.81 ± 11.93

* Tests conducted in the UC Davis Bioenvironmental Engineering Lab, and other tests were conducted by Ward Laboratories Inc. ** Standard deviation was calculated from two independent samples taken from a large batch of each shell. *** Not detected.

After pyrolysis, the kiln lid was kept closed until its temperature reached approximately 280 °C, and the average temperature of the biochar reached approximately 300 °C. Then, the lid was opened while keeping nitrogen flows at 9.44 L min^{-1}, to speed up the cooling process of the crucibles to a temperature of approximately 130–150 °C. The crucibles, with the tile still covered, were removed from the kiln and set aside until their temperature reached ambient temperature. After cooling, the resulting biochar was weighed. Biochar yields from almond and pistachio shells were calculated as percentages of the dry weight of shells placed in each crucible.

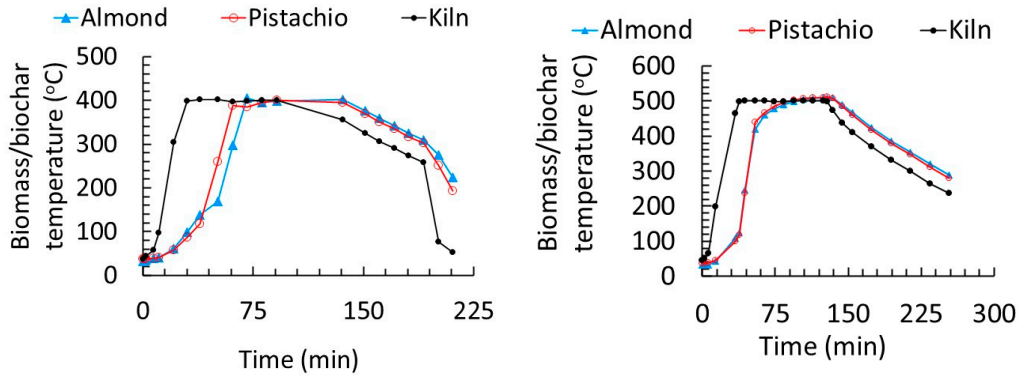

Figure 2. Example temperature profiles during pyrolysis: 400 °C for 90 min (**left**) and 500 °C for 90 min (**right**).

2.5. Analysis of Shells and Biochar

Elemental composition, pH, soluble salts and electrical conductivity (EC) of the produced biochar and biochar extracts were measured by Ward Laboratories Inc. (https://www.wardlab.com/). Mineral content was analyzed using USEPA Method 3050 [28]. Total nitrogen was analyzed using AOAC Method 990.03 [29]. Ammonium nitrogen was analyzed using AOAC Method 973.49 [30]. pH was measured using the method described by McLean [31]. Soluble salts and electrical conductivity (EC) were measured using the method described by Rhoades [32]. The total and volatile solids of shells and biochar were determined according to APHA [33]. Bulk density of the shells and their biochar was determined in duplicate at least and based on the ASABE S269.5 method [34]. A Thermo Fisher Scientific Nicolet iS10 Fourier Transform Infrared Spectroscopy (FTIR) (Waltham, MA, USA), along with a Smart iTR attenuated total reflectance attachment in absorbance mode, was used to perform the FTIR experiments. FTIR measurements were performed in triplicate for each biochar sample, and the average spectrum from the three measurements is presented. Each sample was scanned 64 times at a resolution of 4 cm^{-1}.

2.6. Statistical Analysis

The effects of pyrolysis temperature, residence time, and type of shells and their interactions on biochar yield were statistically analyzed using a full factorial linear model:

$$Y_{ijk} = \mu + S_i + T_j + R_k + (ST)_{ij} + (SR)_{ik} + (TR)_{jk} + (STR)_{ijk} + \varepsilon_{ijk} \quad (8)$$

where Y_{ijk} is the biochar yield under Shell type i, Temperature level j, and Residence time k; μ is the overall mean biochar yield; S_i is the effect of Shell type; T_j is the effect of Temperature; R_k is the effect of Residence time; ST_{ij}, SR_{ik}, and TR_{jk} represent the two-way interaction effects; STR_{ijk} represents the three-way interaction effect; and ε_{ijk} is the random error term.

Analysis of variance (ANOVA) was used to assess the significance of the main effects and interaction terms. The statistical differences were considered significant at $p < 0.05$. Post hoc comparisons were carried out using estimated marginal means (EMMs), with Tukey's adjustment applied to account for multiple comparisons. All pairwise comparisons among the combinations of shell type × pyrolysis temperature × residence time were evaluated. All statistical analyses were conducted using R software (version 4.4.3).

3. Results and Discussion

3.1. Characteristics of Almond and Pistachio Shells

Chemical compositions of almond and pistachio shells are shown in Table 1. Almond shells had higher moisture content and total and organic nitrogen than pistachio shells. Almond shells also contained higher concentrations of Fe, Mn, Zn, S, Ca, Cu, K_2O, P_2O_5, and soluble salts than pistachio shells. The shells of both crops contained comparable concentrations of Na. The pH of pistachio shells was higher than that of almond shells. Almond shells had higher concentrations of soluble salts and ash than pistachio shells. This might be due to the contamination of the shells with soil particles during conventional on-ground harvesting. Pistachio shells had a higher C/N ratio than almond shells. The determined C/N ratio (270.80) was much higher than that (139.44) determined by Açıkalın et al. [9]. Differences in C/N ratios may result from variations in analytical methods and sample preparation. Shell source and cultivar can also influence their chemical composition and C/N ratio. Residual kernel material, hulls, or other contaminants may further contribute to differences from published values.

3.2. Thermogravimetric Analysis

Thermogravimetric analysis results of raw almond and pistachio shells are shown in Figure 3. Almond shells had relatively higher mass losses than pistachio shells in the temperature range of 100–365 °C. At temperatures higher than 365 °C, pistachio shells had greater mass losses than almond shells. The DTG profiles clearly showed the temperature ranges where the major thermal decomposition events occurred for the two biomass types. Following the initial loss of moisture and light volatile compounds below 120 °C, the decomposition of the structural components began. Almond shells showed a broad decomposition region between approximately 250 and 350 °C, which was associated with hemicellulose degradation and overlapped with the main cellulose decomposition. In contrast, pistachio shells showed a more distinct two-stage decomposition between 250 and 400 °C, with a first decomposition stage around 300 °C followed by the main cellulose decomposition at approximately 362 °C. For both samples, the gradual mass loss above 400 °C was associated with the decomposition of the more thermally stable lignin fraction and formation of char. Ma et al. [35] mentioned that thermal decomposition of hemicellulose occurred in the temperature range of 100–365 °C, while cellulose and lignin degradation occurred between 270 and 500 °C. Li et al. [36] mentioned that the main decomposition of almond shells occurred in the temperature range of 200–450 °C, with a char content (fixed carbon) of 20% and a final oxidized ash content of 4.4%, which is comparable to the ash content (5.80%) of the almond shells in this study (Table 1). Debevc et al. [4] found that almond shells lost 15% of their mass at temperatures in the range of 200–300 °C. They also found that a large decrease in weight occurred at 340 °C, which was attributed to thermal degradation of cellulose and lignin.

Thermal degradation of biomass materials depends on the contents of moisture, hemicelluloses, cellulose, and lignin [37–39]. Firstly, dehydration occurs at temperatures less than 120 °C. Decomposition of hemicelluloses occurs at a temperature range of 125 to 250 °C. Then, cellulose degradation occurs at temperatures ranging from 250 to 360 °C. Lastly, lignin degradation occurs at temperatures greater than 450 °C. According to López-Velázquez [39], the pyrolytic cracking process occurs in the temperature range of 125 to 450 °C.

From Figure 3, the remaining mass of almond shells at 400, 450, and 500 °C was 36.0%, 32.5%, and 28.1%, respectively. For pistachio shells, the corresponding remaining masses were 31.2%, 27.6%, and 23.6%, respectively. In comparison, the average yields of biochar from the fixed-bed pyrolyzer at 400, 450, and 500 °C for 60 min were 40.20%, 36.42%, and 35.38%, respectively, for almond shells and 32.58%, 28.76%, and 26.79%, respectively, for

pistachio shells. Relatively greater biochar yields were determined from the fixed-bed pyrolyzer than the TGA. This might be due to better heat transfer in the TGA than in the fixed-bed pyrolyzer.

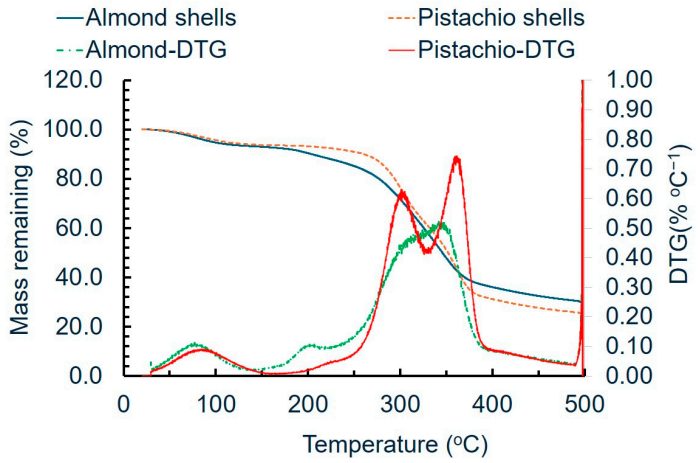

Figure 3. Thermogravimetric analysis results for almond and pistachio shells.

3.3. Pyrolysis Kinetics

The measured and predicted conversions of almond and pistachio shells at different heating rates from 150 to 500 °C are shown in Figures 4 and 5. The average estimated frequency factor (A) and the apparent activation energy (Ea) were determined from the kinetic model (Equation (7)). The frequency factor and activation energy depend on material structure and reactivity, respectively [15]. The activation energy values estimated in the current study are lower than those reported by Rasool et al. [40], who used heating rates of 4.70–4.80 K s^{-1} and obtained values of 153.00 kJ mol^{-1} (Kissinger–Akahira–Sunose), 152.02 kJ mol^{-1} (Ozawa–Flynn–Wall), and 152.73 kJ mol^{-1} (Starink). Using iso-conversional model-free methods, Khan et al. [18] estimated higher activation energies for the pyrolysis of almond shells based on thermogravimetric analysis at temperatures up to 900 °C, at heating rates of 0.17, 0.25, and 0.33 Ks^{-1}. The corresponding average values were 198.45, 204.43, and 204.97 kJ mol^{-1} for the Friedman, Ozawa–Flynn–Wall, and Kissinger–Akahira–Sunose methods, respectively. The differences between the studies might be attributed to the experimental conditions and models employed and differences in feedstock characteristics. Therefore, differences in the estimated activation energies should be interpreted considering both the kinetic approach and the experimental conditions used in each study. It should also be mentioned that lignocellulosic biomass undergoes multiple overlapping reactions involving its different components, making a single-step kinetic model a simplified representation of the overall pyrolysis process that may not capture changes in apparent activation energy with conversion [41,42].

The values of A and E_a were greater for pistachio shells than for almond shells. The greater values of E_a for pistachio shells might be attributed to their harder nature compared to almond shells. For hardwood, softwood pellets, and refuse-derived fuel, Almusafir and Smith [19] mentioned that activation energy values increased with the progress of conversion due to the presence of more stable molecules that are more difficult to break. The estimated E_a values for almond shells were similar at different heating rates. However, in comparison, pistachio shells had higher E_a values at higher heating rates. Main et al. [15] mentioned that the increase in activation energy with an increase in heating rates is attributed to the effect of heat and mass diffusion rather than chemical reactions.

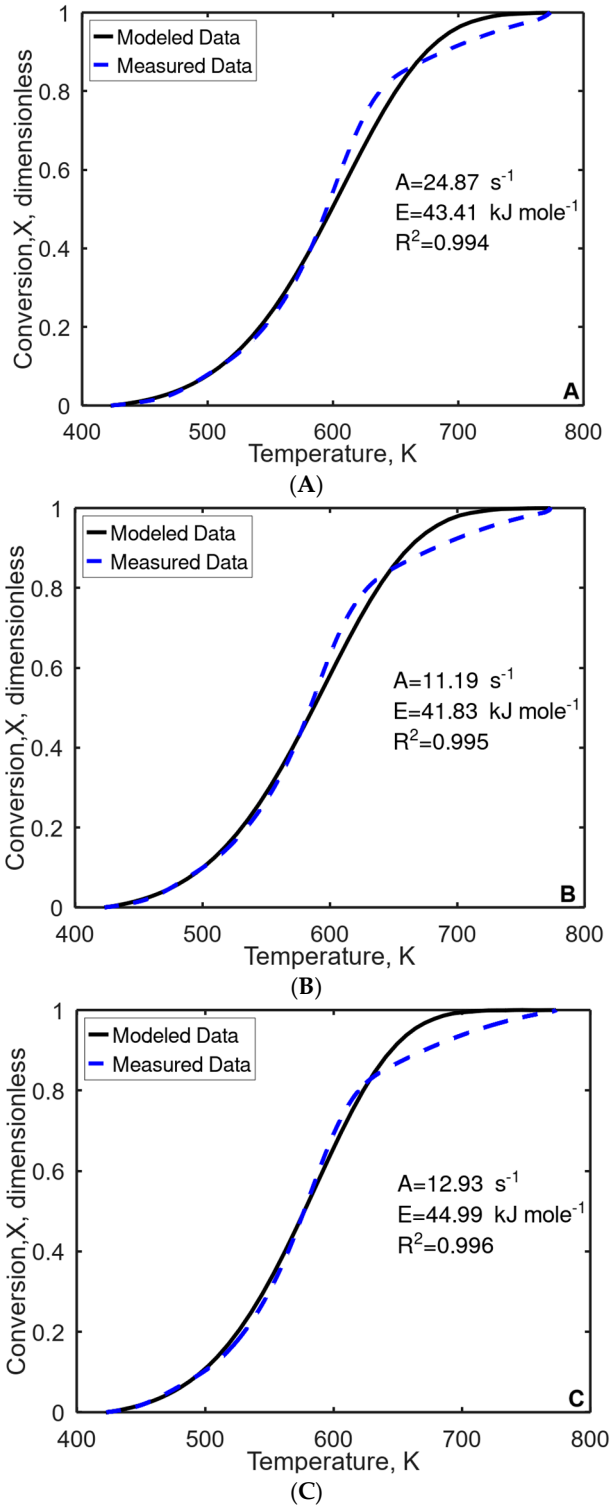

Figure 4. Average measured and predicted conversion of almond shells at heating rates of 0.34 Ks^{-1} (**A**), 0.17 Ks^{-1} (**B**), and 0.08 Ks^{-1} (**C**).

In addition to the duplicate experiments conducted to estimate model parameters, one more TGA test was conducted at each heating rate for both materials. The TGA from the latter test was used to validate the estimated parameters. Results are shown in Figures 4 and 5. From the figures, there is very good agreement ($R^2 \geq 0.994$) between measured and predicted values of conversion for both almond and pistachio shells.

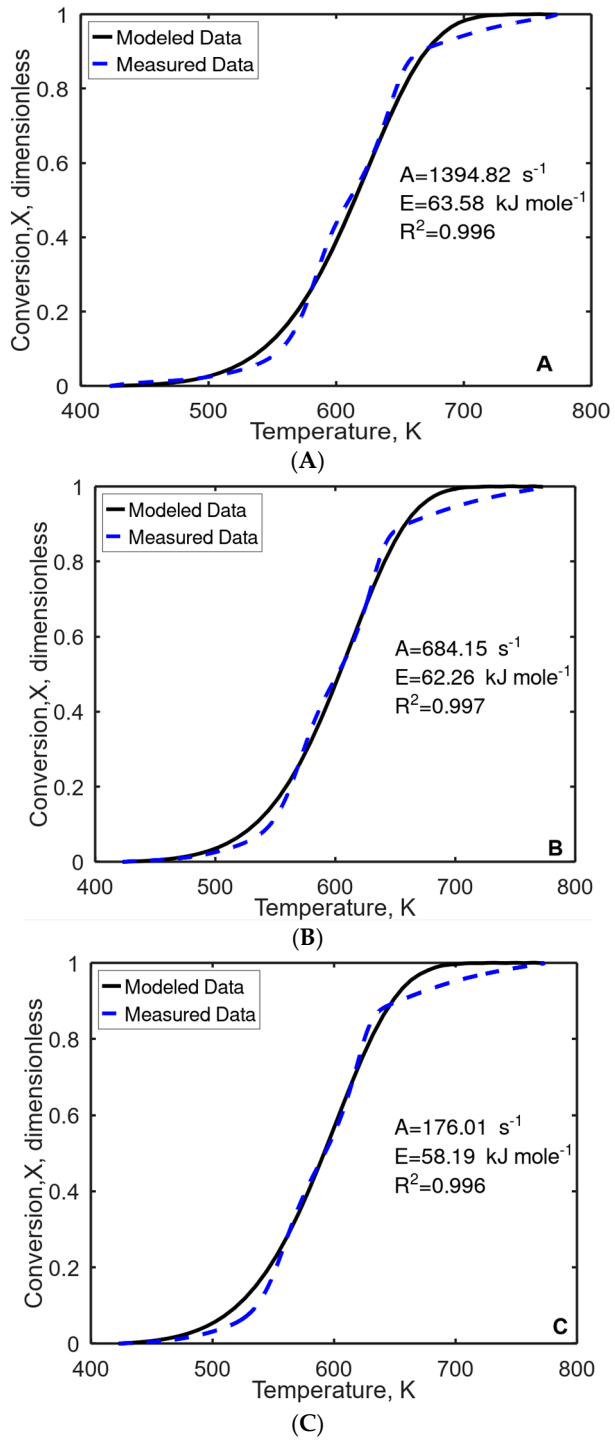

Figure 5. Average measured and predicted conversion of pistachio shells at heating rates of 0.34 Ks^{-1} (**A**), 0.17 Ks^{-1} (**B**), and 0.08 Ks^{-1} (**C**).

3.4. Biochar Yield from the Fixed-Bed Pyrolyzer

For both types of shells, higher biochar yields were obtained at lower pyrolysis temperatures and shorter pyrolysis times (Figure 6A,B). Similar results were obtained for biochar produced from almond shells at comparable pyrolysis temperatures and times [4,7]. Higher yields of biochar were obtained from almond shells than from pistachio shells. This might be due to the higher ash content in the almond shells. This may result from differences in composition and thermal degradation behavior. Their higher ash and soluble salt contents, lower VS/TS ratio, and lower bulk density may contribute to greater resistance to mass loss and retention of more solid residue during pyrolysis. These characteristics may

collectively influence heat and mass transfer and contribute to the higher biochar yield. Sanchez et al. [43] produced biochar from ground pistachio shells and found that after two hours of pyrolysis, biochar yields were 42%, 35%, and 33% at pyrolysis temperatures of 450, 550, and 650 °C, respectively. Using a horizontally placed tubular quartz reactor, Açıkalın et al. [9] determined biochar yields of 30.8% and 22.4% from almond shells at temperatures of 350 and 650 °C, respectively, at a pyrolysis time of 30 min.

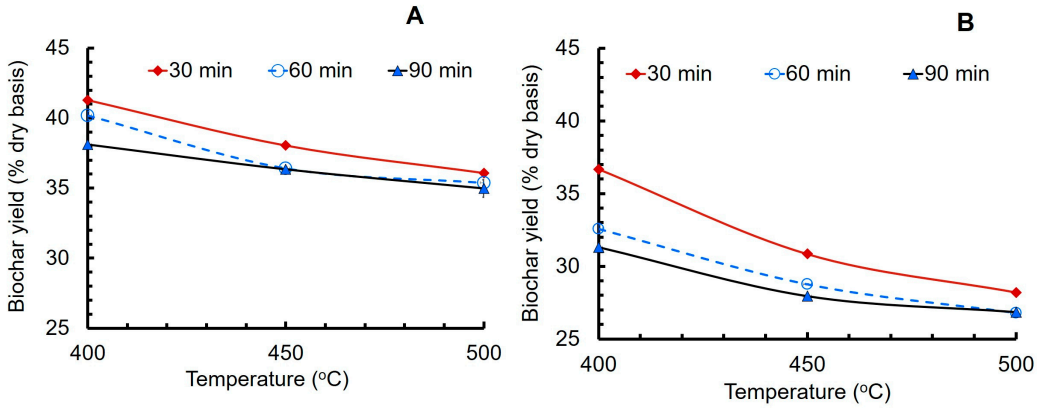

Figure 6. Biochar yields from almond (**A**) and pistachio (**B**) shells. Y error bars are standard deviations between duplicate experiments at each condition.

Statistical analysis revealed that pyrolysis temperature, residence time, shell type, and interactions had significant effects on biochar yield (Table A1). The significant three-way interaction indicates that the effects of pyrolysis temperature and residence time on biochar yield depended on shell type, with yield responses varying across the specific temperature-residence time combinations for almond and pistachio shells. Post hoc comparisons using EMMs further indicated significant differences among pyrolysis conditions and each shell type, with the specific non-significant comparisons presented in Table A2. These findings suggest that both individual factors and their combined effects play an important role in determining biochar yield.

3.5. Elemental Composition of Biochar

The compositions of biochar produced from almond and pistachio shells are shown in Table 2. It should be noted that, because temperature and residence time were not independently varied across all treatments, the observed differences in biochar composition should be interpreted based on the specific temperature–residence time combinations evaluated rather than as independent effects of either factor. Almond shells' biochar generally contained higher contents of N, Ca, K, Mn, Mg, Cu, and Zn than the pistachio shells' biochar. Also, almond shell biochar had a higher pH than that of pistachio shell biochar. The reported standard deviation (SD) values were calculated from two replicate samples, with one sample collected from each of two duplicate crucibles. Thus, the SD values represent variability between the duplicate biochar samples produced in the two crucibles. Samples without reported SD were analyzed using only one sample from the duplicate crucibles due to cost constraints. The large standard deviations observed for Zn and Fe might indicate a large variability among the samples, which may reflect sample heterogeneity and differences in mineral distribution within the biochar. Although contamination cannot be ruled out, no evidence of external contamination was identified during sample preparation and analysis. The bulk density of almond shell biochar was comparable to that of pistachio shell biochar. While total carbon increased at higher temperatures, total nitrogen decreased, particularly for pistachio shells. Increasing pyrolysis temperature may promote carbon enrichment through the loss of volatile hydrogen- and

oxygen-containing compounds, while nitrogen decreases due to the thermal degradation and volatilization of nitrogen-containing compounds [44]. The C/N ratio of almond biochar ranged from 75.90 to 84.75, and pistachio biochar ranged from 72.3 to 215.40. The C/N ratio of the almond biochar was much higher than the values reported in our previous study [7]. This might be due to the C/N ratio in the previous study being based on the organic matter content of biochar rather than the results from using the combustion method in this study. The combustion method directly measures total carbon and nitrogen concentrations, whereas estimating carbon from organic matter content may result in different C/N ratios. Therefore, the difference in C/N ratios between the two studies may be attributed to the different analytical methods used to determine carbon and nitrogen.

Table 2. Chemical characteristics of almond and pistachio biochar.

Shells Type	**Almond**	**Pistachio**	**Almond**	**Pistachio**	**Almond**	**Pistachio**	**Almond**	**Pistachio**
Pyrolysis temperature (°C)	400	400	400 *	400 *	450	450	500	500
Pyrolysis time (min)	30	30	90	90	60	60	90	90
Organic N, % N	0.85 ± 0.00 **	0.90 ± 0.21	0.91	0.59	0.92 ± 0.02	0.39 ± 0.00	0.88 ± 0.01	0.45 ± 0.01
Ammonium, % N	0.00 ± 0.00	0.00 ± 0.00	0.01	0.00	0.00 ± 0.00	0.00 ± 0.00	0.00 ± 0.00	0.00 ± 0.00
Total N, % N	0.86 ± 0.01	0.90 ± 0.21	0.92	0.59	0.92 ± 0.03	0.40 ± 0.01	0.88 ± 0.01	0.45 ± 0.01
Phosphorus, % as P_2O_5	0.18 ± 0.11	0.38 ± 0.18	0.11	0.15	0.24 ± 0.15	0.15 ± 0.09	0.35 ± 0.02	0.33 ± 0.01
K, % as K_2O	4.25 ± 0.59	0.93 ± 0.10	4.01	0.87	4.82 ± 0.82	0.86 ± 0.17	6.14 ± 0.01	1.21 ± 0.16
Sulfur, % S	0.03 ± 0.01	0.03 ± 0.01	0.02	0.01	0.03 ± 0.01	0.02 ± 0.01	0.03 ± 0.00	0.02 ± 0.00
Calcium, % Ca	0.47 ± 0.05	0.20 ± 0.03	0.53	0.14	0.60 ± 0.04	0.16 ± 0.04	0.60 ± 0.07	0.17 ± 0.01
Magnesium, % Mg	0.14 ± 0.01	0.08 ± 0.01	0.15	0.06	0.18 ± 0.01	0.06 ± 0.02	0.16 ± 0.03	0.06 ± 0.01
Sodium, % Na	0.03 ± 0.03	0.02 ± 0.02	0.01	0.01	0.03 ± 0.02	0.02 ± 0.02	0.04 ± 0.00	0.04 ± 0.00
Zinc, ppm Zn	111.89 ± 136.17	47.49 ± 54.43	45.56	41.71	30.18 ± 23.02	13.18 ± 11.42	11.45 ± 4.45	4.15 ± 1.48
Iron, ppm Fe	520.25 ± 241.90	39.83 ± 0.52	621.20	28.70	1217.66 ± 389.99	39.18 ± 21.11	1065.85 ± 641.42	51.35 ± 2.76
Manganese, ppm Mn	25.17 ± 2.59	8.29 ± 5.36	26.59	4.83	35.00 ± 4.81	3.65 ± 0.64	36.20 ± 8.63	5.45 ± 1.34
Copper, ppm Cu	10.77 ± 2.17	5.54 ± 0.76	11.53	4.27	14.50 ± 2.83	3.07 ± 0.47	13.40 ± 3.54	4.00 ± 0.14
Boron, ppm B	98.87 ± 3.30	10.41 ± 1.29	92.77	10.61	109.87 ± 4.00	9.16 ± 0.91	117.70 ± 0.28	12.70 ± 1.98
Soluble salts, mS/cm	28.63 ± 1.05	1.45 ± 0.66	43.97	N.D.	51.64 ± 14.96	3.36 ± 1.44	52.74 ± 3.69	4.39 ± 0.74
pH	9.50 ± 0.14	7.45 ± 0.78	10.10	N.D.	9.75 ± 0.49	8.85 ± 0.07	9.30 ± 0.00	8.95 ± 0.07
Moisture, %	5.13 ± 0.27	3.45 ± 0.23	5.65	3.36	5.42 ± 0.38	3.89 ± 0.04	5.00 ± 0.21	3.13 ± 0.08
Dry matter, %	94.87 ± 0.27	96.55 ± 0.23	94.35	96.64	94.58 ± 0.38	96.11 ± 0.04	95.01 ± 0.21	96.87 ± 0.08
Total carbon, % C	70.15 ± 0.91	76.85 ± 0.14	73.02	81.08	73.91 ± 1.49	85.07 ± 0.59	74.12 ± 4.82	84.45 ± 8.17
Total C/N ratio	81.60 ± 0.28	87.80 ± 20.51	75.90	72.30	80.40 ± 4.10	215.40 ± 2.40	84.75 ± 6.15	188.05 ± 24.11
VS/TS, %	91.45 ± 0.81	96.98 ± 0.91	87.77 ± 2.29	97.95 ± 0.27	84.79 ±1.04	97.91 ± 0.37	88.46 ± 2.02	98.00 ± 0.03
Bulk density, kg/m^3	151.06 ± 8.22	N.D. ***	157.08 ±3.07	160.43 ± 2.23	158.26 ±0.98	154.32 ± 1.11	153.72± 3.07	144.66 ± 0.28

* One sample was analyzed. ** Standard deviation between duplicate biochar samples produced in two crucibles under the same pyrolysis temperature and time. *** N.D., not determined.

In addition, pistachio shells' biochar contained higher VS/TS values than almond shells. For almond shells, increasing pyrolysis time from 30 to 90 min at 400 °C led to decreased VS/TS values. For other temperatures and pyrolysis times, VS/TS values remained relatively similar. For pistachio shells, VS/TS values were comparable for different temperatures and times. Moreover, almond biochar generally showed higher pH than pistachio biochar under matched temperature–residence time conditions. The biochar samples had higher pH values than the raw shells (Table 1), probably due to the reduction in acidic organic compounds [8]. Sodium concentration was comparable in both types of biochar. Under matched temperature and residence time conditions, almond biochar had higher soluble salts than the corresponding pistachio biochars. The high soluble-salt content of almond biochar may increase soil electrical conductivity and potentially cause phytotoxicity at high application rates, particularly for salt-sensitive crops when biochar is used as a soil amendment for carbon sequestration. Therefore, application rates should be carefully considered based on the biochar's salt content and crop tolerance.

3.6. Fourier Transform Infrared Spectroscopy (FTIR)

Infrared spectra of almond and pistachio shell biochar are shown in Figures 7 and 8. The peaks in the range of 790–870 cm^{-1} can be associated with out-of-plane C-H bending on aromatic structures, with possible contributions from C-H bending variations in aliphatic groups such as CH_2 [45]. The temperature of pyrolysis affects the absorption intensity and position of several bands, reflecting changes in the chemical structure of the biochars. The peak at 974 cm^{-1} can be related to the C-H bending mode in alkyl compounds. The peaks at 1000–1026 cm^{-1} correspond to C–O and C–O–C stretching vibrations associated with oxygen-containing structures derived from lignocellulosic components. This peak increased in intensity at higher pyrolysis temperatures, especially for the almond samples, which may indicate relative enrichment of aromatic structures and progressive carbonization. The peak at 1100–1235 cm^{-1} is associated with C-O stretching vibrations in alcohols, phenols, ethers, and other oxygen-containing functional groups. The peaks in the range from 1030 to 1160 cm^{-1} represent oxygenated groups of cellulose [46,47]. Chen et al. [46] mentioned that the thermal destruction of cellulose, ester C=O, aliphatic alkyl, aromatic C=O, and -OH groups results in exposing the aromatic cores derived from lignin, and these remain at high temperatures of pyrolysis. This transformation is consistent with the progressive degradation of thermally labile oxygenated and aliphatic structures and the relative enrichment of more condensed aromatic structures at higher pyrolysis temperatures. The peaks in the range of 1250 cm^{-1} can be related to organic phosphates (P=O stretch). The peaks in the 1367–1392 cm^{-1} range correspond to the bending vibration of C-H in methyl groups ($-CH_3$). The peaks in the 1567–1620 cm^{-1} range can be attributed to aromatic C=C stretching and skeletal vibrations of aromatic structures. The presence or relative increase in these aromatic bands at higher pyrolysis temperatures indicates increased carbonization and formation of more stable aromatic structures. The peaks in the range of 2020–2365 cm^{-1} may correspond to weak C≡C or C≡N stretching vibrations [48]. The peaks in the range of 2800–3000 cm^{-1} correspond to C-H stretches in alkanes. Apaydin-Varol et al. [49] mentioned that biochar produced from pistachio shells at 300 and 400 °C had very weak bands at about 2850 cm^{-1}, indicating C–H stretching vibrations in the CH_2 group. The peak at 3170–3382 cm^{-1} corresponds to free O-H stretches in phenols or alcohols. This peak decreased in size with an increase in temperature and pyrolysis times. This was most likely due to continued degradation of cellulose and lignin in the samples that produced more hydrophobic materials. The decrease in O–H intensity indicates the loss of hydroxyl-containing and other oxygenated functional groups during pyrolysis, which is associated with increasing carbonization and greater chemical stability of the resulting biochar. The peak in the range 3610–3630 cm^{-1} also corresponds to free O-H stretches in phenols, carboxylic acids, or alcohols [45,48].

Overall, the reduction in oxygen-containing groups and enrichment of aromatic structures with increasing pyrolysis temperature may indicate greater biochar stability, while the remaining functional groups may provide reactive sites for nutrient interactions and contaminant adsorption [50]. Thus, pyrolysis temperature influences biochar stability and surface reactivity, and therefore its potential applications in soil amendment, carbon sequestration, and contaminant removal.

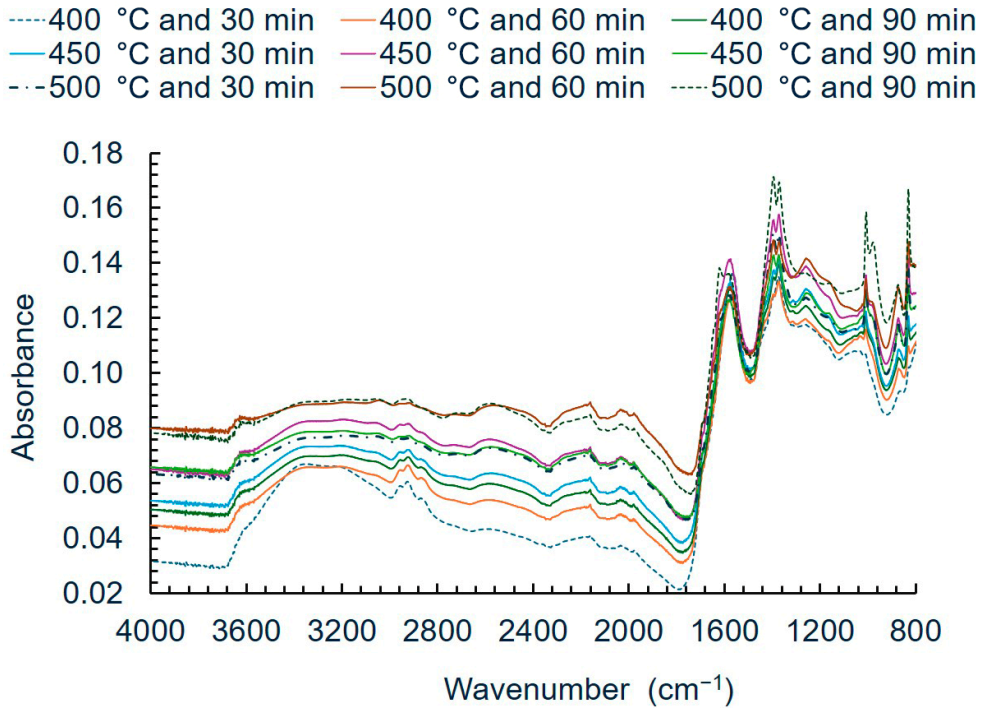

Figure 7. FTIR spectra of almond shell biochars.

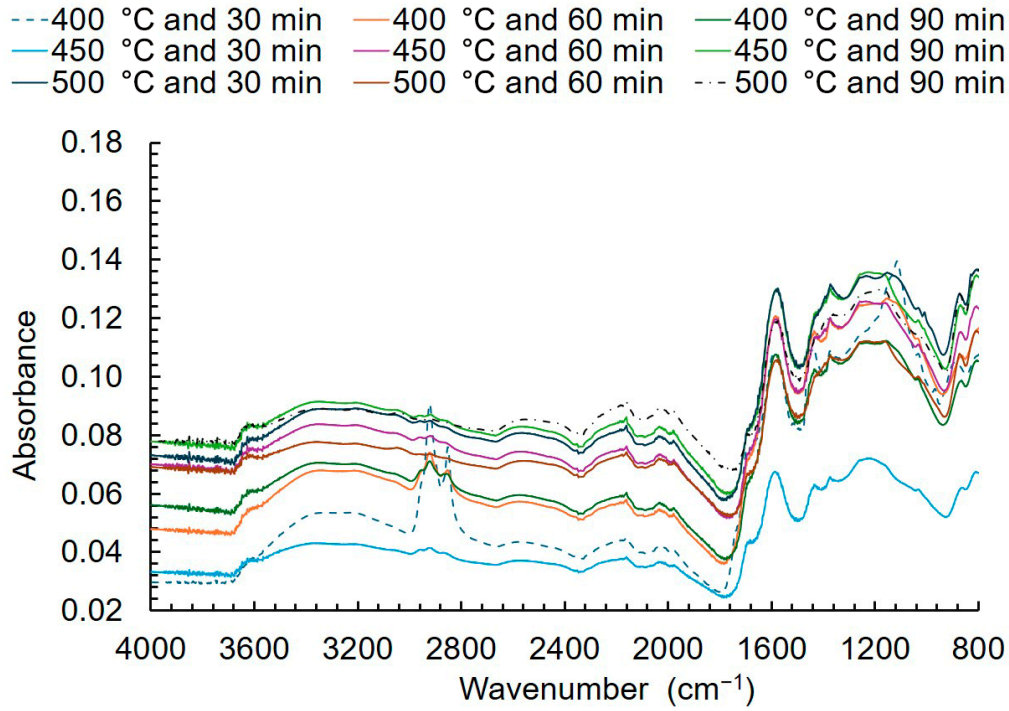

Figure 8. FTIR spectra of pistachio shell biochars.

4. Conclusions

Higher yields of biochar were obtained from almond shells than from pistachio shells. Biochar yield from both materials decreased with an increase in pyrolysis temperatures from 400 to 450 °C and time from 30 to 60 min. However, the yield was relatively similar at 400 and 500 °C, and at pyrolysis times of either 60 or 90 min. Biochar yield was significantly influenced by pyrolysis temperature and residence time, shell type, and their interactions. The significant three-way interaction indicated that these factors should not be interpreted as independent trends. Biochar produced from almond shells had some different functional

groups than that of the biochar from pistachio shells. A first-order kinetic model was found to adequately describe the kinetic degradation of both almond and pistachio shells. The estimated frequency factor and the apparent activation energy were greater for pistachio shells than almond shells. Validation of the model showed a very good agreement between predicted and measured conversion of both shells at 500 °C.

Overall, the results provide useful information for understanding the differences in pyrolysis behavior of almond and pistachio shells and for selecting appropriate pyrolysis conditions for biochar production from these agricultural residues. A limitation of this study was that only one sample of each shell type was evaluated, which limited quantitative assessment of the relationships between feedstock characteristics and pyrolysis behavior. Future studies should evaluate multiple samples collected from different processors to account for variability in shell characteristics and further investigate the relationships between shell composition and the chemical and physicochemical properties of the produced biochars. In addition, optimization of pyrolysis parameters is needed to improve biochar yield and ensure consistent biochar properties across different shell types and sources. Such studies would provide a better basis for selecting appropriate biochars for different applications.

Author Contributions: H.M.E.M., F.M., and B.-S.C. conception, research design, funding acquisition. H.M.E.M., data analysis, kinetic modeling, and writing the first draft. A.E., experimentation of biochar production experiments, and formatting the manuscript. B.-S.C. and T.C., FTIR analyses. Z.M. and W.H.-C., TGA analyses. R.Z., supervision and project administration. All authors have read and agreed to the published version of the manuscript.

Funding: The research leading to these results received funding from the Resnick Agricultural Innovation Research Fund.

Institutional Review Board Statement: Not applicable.

Informed Consent Statement: Not applicable.

Data Availability Statement: The datasets presented in this study are available from the corresponding author upon reasonable request.

Acknowledgments: We would like to thank the Resnick Agricultural Innovation Research Fund for providing financial support for this study. We also sincerely thank Victor Duraj for his assistance with the transportation and setup of the fixed-bed pyrolyzer.

Conflicts of Interest: The authors declare no conflicts of interest. The funders had no role in the design of the study; in the collection, analyses, or interpretation of data; in the writing of the manuscript; or in the decision to publish the results.

Abbreviations

TGA	Thermogravimetric Analysis
FTIR	Fourier Transform Infrared Spectroscopy
SDGs	Sustainable Development Goals
ANOVA	Analysis of Variance
EMMS	Estimated Marginal Means (EMMS)
C/N Ratio	Carbon to Nitrogen Ratio
TS	Total Solids
VS	Volatile Solids

Appendix A

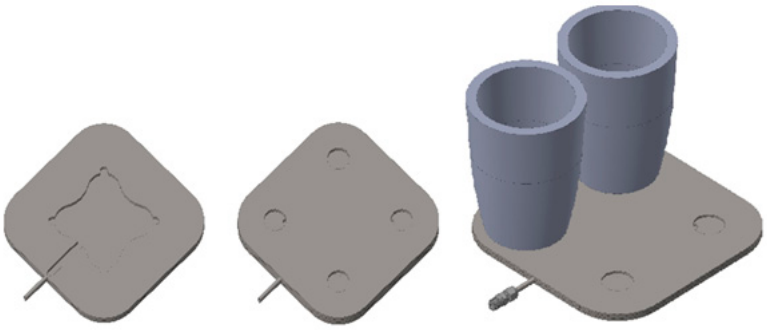

Figure A1. A manifold for nitrogen distribution for biochar production containers.

Appendix B

Table A1. Results of ANOVA test for biochar yields.

Source of Variance	df	Sum Squares	Mean Squares	F Value	Pr (>F)
Temperature	2	176.62	88.31	2193.38	0.00
Residence time	2	43.29	21.65	537.61	0.00
Shells type	1	497.74	497.74	12,362.70	0.00
Temperature: residence time	4	9.65	2.41	59.89	0.00
Temperature: shells type	2	5.66	2.83	70.23	0.00
Residence time: shells type	2	3.39	1.69	42.06	2.00×10^{-7}
Temperature: residence time: shells type	4	2.44	0.61	15.15	1.38×10^{-5}
Residuals	18	0.73	0.04	NA	NA

Table A2. Pairwise comparisons with non-significant differences ($p \geq 0.05$).

Contrast	Estimate	SE	df	t.Ratio	*p*.Value
Pistachio (400 °C, 30 min) − Almond (500 °C, 30 min)	0.59	0.20	18	2.94	0.32
Pistachio (400 °C, 30 min) − Almond (450 °C, 60 min)	0.27	0.20	18	1.32	0.99
Pistachio (400 °C, 30 min) − Almond (450 °C, 90 min)	0.35	0.20	18	1.72	0.94
Almond (450 °C, 30 min) − Almond (400 °C, 90 min)	−0.03	0.20	18	−0.15	1.00
Pistachio (450 °C, 30 min) − Pistachio (400 °C, 90 min)	−0.46	0.20	18	−2.27	0.69
Almond (500 °C, 30 min) − Almond (450 °C, 60 min)	−0.33	0.20	18	−1.62	0.96
Almond (500 °C, 30 min) − Almond (500 °C, 60 min)	0.71	0.20	18	3.51	0.13
Almond (500 °C, 30 min) − Almond (450 °C, 90 min)	−0.25	0.20	18	−1.22	1.00
Pistachio (500 °C, 30 min) − Pistachio (450 °C, 60 min)	−0.56	0.20	18	−2.79	0.39
Pistachio (500 °C, 30 min) − Pistachio (450 °C, 90 min)	0.27	0.20	18	1.35	0.99
Almond (450 °C, 60 min) − Almond (450 °C, 90 min)	0.08	0.20	18	0.40	1.00
Almond (500 °C, 60 min) − Almond (500 °C, 90 min)	0.41	0.20	18	2.04	0.82
Pistachio (500 °C, 60 min) − Pistachio (500 °C, 90 min)	−0.06	0.20	18	−0.27	1.00

References

1. California Department of Food and Agriculture. *2022–2023 California Agricultural Statistics Review*; California Department of Food and Agriculture: Sacramento, CA, USA, 2024. Available online: https://www.cdfa.ca.gov/Statistics/PDFs/2022-2023_california_agricultural_statistics_review.pdf (accessed on 1 May 2026).
2. Lua, A.C.; Yang, T.; Guo, J. Effects of pyrolysis conditions on the properties of activated carbons prepared from pistachio-nut shells. *J. Anal. Appl. Pyrolysis* **2004**, *72*, 279–287. [CrossRef]
3. Babu, S.; Singh, R.; Yadav, D.; Rathore, S.S.; Yadav, D.K.; Kumar, S.; Wani, O.A.; Venkatramanan, V. Agricultural waste-derived biochar in a circular bioeconomy: Implications for food security, climate mitigation, and sustainable development goals. *Next Sustain.* **2026**, *7*, 100326. [CrossRef]

4. Debevc, S.; Weldekidan, H.; Snowdon, M.R.; Vivekanandhan, S.; Wood, D.F.; Misra, M.; Mohanty, A.K. Valorization of almond shell biomass to biocarbon materials: Influence of pyrolysis temperature on their physicochemical properties and electrical conductivity. *Carbon Trends* **2022**, *9*, 100214. [CrossRef]
5. McCaffrey, Z.; Thy, P.; Long, M.; Oliveira, M.; Wang, L.; Torres, L.; Aktas, T.; Chiou, B.S.; Orts, W.; Jenkins, B.M. Air and steam gasification of almond biomass. *Front. Energy Res.* **2019**, *7*, 84. [CrossRef]
6. Ungureanu, N.; Vlăduț, N.-V.; Biriș, S.-Ș.; Gheorghiță, N.-E.; Ionescu, M. Biomass pyrolysis pathways for renewable energy and sustainable resource recovery: A critical review of processes, parameters, and product valorization. *Sustainability* **2025**, *17*, 7806. [CrossRef]
7. El Mashad, H.M.; Edalati, A.; Zhang, R.; Jenkins, B.M. Production and characterization of biochar from almond shells. *Clean. Technol.* **2022**, *4*, 854–864. [CrossRef]
8. Gezahegn, S.; Sain, M.; Thomas, S.C. Variation in feedstock wood chemistry strongly influences biochar liming potential. *Soil Syst.* **2019**, *3*, 26. [CrossRef]
9. Açıkalın, K.; Karaca, F.; Bolat, E. Pyrolysis of pistachio shell: Effects of pyrolysis conditions and analysis of products. *Fuel* **2012**, *95*, 169–177. [CrossRef]
10. Wang, L.; Lei, H.; Liu, J.; Buc, Q. Thermal decomposition behavior and kinetics for pyrolysis and catalytic pyrolysis of Douglas fir. *RSC Adv.* **2018**, *8*, 2196–2202. [CrossRef] [PubMed]
11. Shrivastava, D.K.; Singh, A.K.; Chakraborty, J.P. Model-free isoconversional methods to determine the intrinsic kinetics and thermodynamic parameters during pyrolysis of boiled banana peel: Influence of inorganic species. *Bioresour. Technol. Rep.* **2023**, *24*, 101676. [CrossRef]
12. Slopiecka, K.; Bartocci, P.; Fantozzi, F. Thermogravimetric analysis and kinetic study of poplar wood pyrolysis. *Appl. Energy* **2012**, *97*, 491–497. [CrossRef]
13. Khawam, A. Application of Solid State-Kinetics to Desolvation Reactions. Ph.D. Thesis, University of Iowa, Iowa City, IA, USA, 2007.
14. Fischer, O.; Lemaire, R.; Bensakhria, A. Thermogravimetric analysis and kinetic modeling of the pyrolysis of different biomass types by means of model fitting, model free and network modeling approaches. *J. Therm. Anal. Calorim.* **2024**, *149*, 10941–10963. [CrossRef] [PubMed]
15. Mian, I.; Li, X.; Jian, Y.; Dacres, O.D.; Zhong, M.; Liu, J.; Ma, F.; Rahman, N. Kinetic study of biomass pellet pyrolysis by using distributed activation energy model and Coats–Redfern methods and their comparison. *Bioresour. Technol.* **2019**, *294*, 122099. [CrossRef] [PubMed]
16. Xiao, R.; Yang, W.; Cong, X.; Dong, K.; Xu, J.; Wang, D.; Yang, X. Thermogravimetric analysis and reaction kinetics of lignocellulosic biomass pyrolysis. *Energy* **2020**, *202*, 117537. [CrossRef]
17. Ceylan, S.; Topçu, Y. Pyrolysis kinetics of hazelnut husk using thermogravimetric analysis. *Bioresour. Technol.* **2014**, *156*, 182–188. [CrossRef] [PubMed]
18. Khan, A.; Saeed, S.; Pervaiz, E.; Khoja, A.H.; Naqvi, S.R.; Saeed, S.; Ali, I. Comprehensive investigation of almond shells pyrolysis using advanced predictive models. *Renew. Energy* **2024**, *227*, 120568. [CrossRef]
19. Almusafir, R.; Smith, J.D. Thermal decomposition and kinetic parameters of three biomass feedstocks for the performance of the gasification process using a thermogravimetric analyzer. *Energies* **2024**, *17*, 396. [CrossRef]
20. Vyazovkin, S.; Chrissafis, K.; Di Lorenzo, M.L.; Koga, N.; Pijolat, M.; Roduit, B.; Sbirrazzuoli, N.; Sunol, J.J. ICTAC kinetics committee recommendations for collecting experimental thermal analysis data for kinetic computations. *Thermochim. Acta* **2014**, *590*, 1–23. [CrossRef]
21. Vyazovkin, S.; Burnham, A.K.; Criado, J.M.; Pérez-Maqueda, L.A.; Popescu, C.; Sbirrazzuoli, N. ICTAC kinetics committee recommendations for performing kinetic computations on thermal analysis data. *Thermochim. Acta* **2011**, *520*, 1–19. [CrossRef]
22. Flynn, H.A. General differential technique for the determination of parameters. *J. Therm. Anal.* **1991**, *37*, 293–305. [CrossRef]
23. Kissinger, H.E. Reaction kinetics in differential thermal analysis. *Anal. Chem.* **1957**, *29*, 1702–1706. [CrossRef]
24. Eaton, J.W.; Bateman, D.; Hauberg, S.; Wehbring, R. *GNU Octave Version 10.1.0 Manual: A High-Level Interactive Language for Numerical Computations*; GNU Project; Network Theory Limited: Bristol, UK, 2025.
25. Gao, Y.; Chen, X.; Zhang, J.; Yan, N. Chitin-derived mesoporous, nitrogen-containing carbon for heavy-metal removal and styrene epoxidation. *ChemPlusChem* **2015**, *80*, 1556–1564. [CrossRef] [PubMed]
26. Wang, S.; Zhang, H.; Huang, H.; Xiao, R.; Li, R.; Zhang, Z. Influence of temperature and residence time on characteristics of biochars derived from agricultural residues: A comprehensive evaluation. *Process Saf. Environ. Prot.* **2020**, *139*, 218–229. [CrossRef]
27. Suman, S.; Panwar, D.S.; Gautam, S. Characterization of biochars produced from pyrolysis of pelletized agricultural residues. *Renew. Sustain. Energy Rev.* **2016**, *64*, 187–194. [CrossRef]
28. USEPA. Method 3050: Acid Digestion of Sediments, Sludges, and Soils. In *Test Methods for Evaluating Solid Waste, Physical/Chemical Methods (SW-846)*, 3rd ed.; U.S. Environmental Protection Agency: Washington, DC, USA, 1986.

29. AOAC International. Official Method 990.03: Protein (Crude) in Animal Feed—Combustion Method. In *Official Methods of Analysis of AOAC International*; AOAC International: Gaithersburg, MD, USA, 2006.
30. AOAC International. Official Method 973.49: Ammonium Nitrogen in Water. In *Official Methods of Analysis of AOAC International*; AOAC International: Gaithersburg, MD, USA, 1998.
31. McLean, E.O. Soil pH and Lime Requirement. In *Methods of Soil Analysis, Part 2: Chemical and Microbiological Properties*, 2nd ed.; Page, A.L., Ed.; Agronomy Monograph No. 9; American Society of Agronomy and Soil Science Society of America: Madison, WI, USA, 1982; pp. 199–223.
32. Rhoades, J.D. Soluble Salts. In *Methods of Soil Analysis, Part 2: Chemical and Microbiological Properties*, 2nd ed.; Page, A.L., Ed.; Agronomy Monograph No. 9; American Society of Agronomy and Soil Science Society of America: Madison, WI, USA, 1982; pp. 167–179.
33. APHA. *Standard Methods for the Examination of Water and Wastewater*, 23rd ed.; American Public Health Association: Washington, DC, USA, 2017.
34. ASABE. *ASAE S269.5 (R2021): Densified Products for Bulk Handling—Definitions and Method*; American Society of Agricultural and Biological Engineers: St. Joseph, MI, USA, 2012.
35. Ma, Z.; Chen, D.; Gu, J.; Bao, B.; Zhang, Q. Determination of pyrolysis characteristics and kinetics of palm kernel shell using TGA–FTIR and model-free integral methods. *Energy Convers. Manag.* **2015**, *89*, 251–259. [CrossRef]
36. Li, X.; Liu, Y.; Hao, J.; Wang, W. Study of almond shell characteristics. *Materials* **2018**, *11*, 1782. [CrossRef] [PubMed]
37. Yang, H.; Yan, R.; Chen, H.; Zheng, C.; Lee, D.H.; Liang, D.T. In-depth investigation of biomass pyrolysis based on three major components: Hemicellulose, cellulose and lignin. *Energy Fuels* **2006**, *20*, 388–393. [CrossRef]
38. Zapata, B.; Balmaseda, J.; Fregoso-Israel, E.; Torres-García, E. Thermo-kinetics study of orange peel in air. *J. Therm. Anal. Calorim.* **2009**, *98*, 309–315. [CrossRef]
39. López-Velázquez, M.; Santes, V.; Balmaseda, J.; Torres-García, E. Pyrolysis of orange waste: A thermo-kinetic study. *J. Anal. Appl. Pyrolysis* **2013**, *99*, 170–177. [CrossRef]
40. Rasool, T.; Najar, I.; Srivastava, V.C.; Pandey, A. Pyrolysis of almond (*Prunus amygdalus*) shells: Kinetic analysis, modelling, energy assessment and technical feasibility studies. *Bioresour. Technol.* **2021**, *337*, 125466. [CrossRef] [PubMed]
41. Wang, S.; Dai, G.; Yang, H.; Luo, Z. Lignocellulosic biomass pyrolysis mechanism: A state-of-the-art review. *Prog. Energy Combust. Sci.* **2017**, *62*, 33–86. [CrossRef]
42. Wu, W.; Mei, Y.; Zhang, L.; Liu, R.; Cai, J. Effective activation energies of lignocellulosic biomass pyrolysis. *Energy Fuels* **2014**, *28*, 3916–3923. [CrossRef]
43. Sanchez, E.; Zabaleta, R.; Navas, A.L.; Torres-Sciancalepore, R.; Fouga, G.; Fabani, M.P.; Rodriguez, R.; Mazza, G. Assessment of pistachio shell-based biochar application in the sustainable amendment of soil and its performance in enhancing bell pepper (*Capsicum annuum* L.) growth. *Sustainability* **2024**, *16*, 4429. [CrossRef]
44. Jassal, R.S.; Johnson, M.S.; Molodovskaya, M.; Black, T.A.; Jollymore, A.; Sveinson, K. Nitrogen enrichment potential of biochar in relation to pyrolysis temperature and feedstock quality. *J. Environ. Manag.* **2015**, *152*, 140–144. [CrossRef] [PubMed]
45. Coates, J. Interpretation of infrared spectra, a practical approach. *Encycl. Anal. Chem.* **2000**, *12*, 10815–10837.
46. Chen, B.; Zhou, D.; Zhu, L. Transitional adsorption and partition of nonpolar and polar aromatic contaminants by biochars of pine needles with different pyrolytic temperatures. *Environ. Sci. Technol.* **2008**, *42*, 5137–5143. [CrossRef] [PubMed]
47. Bustin, R.M.; Guo, Y. Abrupt changes (jumps) in reflectance values and chemical compositions of artificial charcoals and inertinite in coals. *Int. J. Coal Geol.* **1999**, *38*, 237–260. [CrossRef]
48. Chemistry LibreTexts. Infrared Spectroscopy Absorption Table. LibreTexts. Available online: https://chem.libretexts.org/Ancillary_Materials/Reference/Reference_Tables/Spectroscopic_Reference_Tables/Infrared_Spectroscopy_Absorption_Table (accessed on 1 June 2026).
49. Apaydin-Varol, E.; Putun, E.; Putun, A.E. Slow pyrolysis of pistachio shell. *Fuel* **2007**, *86*, 1892–1899. [CrossRef]
50. Tomczyk, A.; Sokołowska, Z.; Boguta, P. Biochar physicochemical properties: Pyrolysis temperature and feedstock kind effects. *Rev. Environ. Sci. Bio/Technol.* **2020**, *19*, 191–215. [CrossRef]